Journal of Magnetic Resonance 230 (2013) 84–87

Contents lists available at SciVerse ScienceDirect

Journal of Magnetic Resonance

journal homepage: www.elsevier.com/locate/jmr

Superconducting microstrip resonator for pulsed ESR of thin films

O.W.B. Benningshof [a,b,*], H.R. Mohebbi [a,c], I.A.J. Taminiau [a], G.X. Miao [a,c], D.G. Cory [a,d,e]

[a] Institute for Quantum Computing, Waterloo, ON, Canada
[b] Department of Physics, University of Waterloo, Waterloo, ON, Canada
[c] Department of Electrical and Computer Engineering, University of Waterloo, Waterloo, ON, Canada
[d] Perimeter Institute for Theoretical Physics, Waterloo, ON, Canada
[e] Department of Chemistry, University of Waterloo, Waterloo, ON, Canada

ARTICLE INFO

Article history:
Received 17 August 2012
Revised 24 January 2013
Available online 5 February 2013

Keywords:
EPR
Superconducting resonator
Cavity quantum electrodynamics
Strong coupling
Nutation spectroscopy

ABSTRACT

This article describes a superconducting microstrip resonator operating at 9.5 GHz (X-band) that is specially designed for pulsed ESR on thin films. A novel configuration consisting of an array of half-wave length microstrip transmission lines generates a uniform magnetic field over a 2-D region of $100 \times 1000\ \mu m^2$ with field homogeneity better than 5×10^{-2}. Using the device, we demonstrate strong coupling of the resonator to an electron spin ensemble and pulsed ESR on Si:P.

1. Introduction

Electron spin resonance (ESR) is a powerful technique in chemistry and materials science and has increasingly been used to generate control sequences for quantum information processing [1]. Improved sensitivity for thin film samples would benefit all of these. To observe small ensembles with high signal-to-noise ratio (SNR) one needs to realize a high Q resonator, have high spin polarization, and tailor the microwave magnetic field of the resonator to the geometry of the sample. Here we introduce a new superconducting resonator that is optimized for the study of 2-D samples.

High resolution ESR benefits from having both a homogeneous external field B_0 and a uniform microwave field B_1. The latter improves sensitivity and simplifies the spin dynamics. Microwave cavities can fulfill these requirements, however their filling factor is small for thin film samples. The development of superconducting planar coils [2,3] and coplanar waveguide (CPW) resonators [4–11] have increased the filling factor significantly, but their B_1 fields are not uniform over a broad 2-D region necessary to study thin films.

Here we report a superconducting microstrip resonator operating at X-band frequencies, based on a novel design of half-wave microstrip transmission lines. An array of microstrip lines provide a high Q resonance at the desired frequency, which generates an in-plane uniform magnetic field suitable for pulsed ESR experiments on thin films. The performance, high sensitivity and small mode volume are verified by demonstrating strong coupling of the resonator to an ensemble of electron spins in perchlorotriphenylmethyl (PTM) and by performing pulsed ESR of a phosphorus doped silicon sample Si:P.

2. The microstrip resonator

Schematic of the microstrip resonator is shown in Fig. 1. A custom designed, in-phase 1–4 power splitter couples the microwave $\lambda/2$ microstrip line resonator. The coupling strength is controlled by coupling the splitters capacitively to the strip lines. The power splitter was designed to maintain impedance matching for maximum power transfer. The length of the $\lambda/2$-resonator was chosen to have a fundamental resonance frequency ω_r (on a sapphire substrate) of 9.5 GHz. The design ensures that all lines resonate in phase. By optimizing the height of the sample above the resonator, the sample experiences a magnetic field with high in-plane uniformity (see Fig. 2). Simulations (Ansoft HFSS [12]) show a magnetic field homogeneity of $\sim 10^{-2}$ (for a range of 100 μm) at 100 μm above the resonator. The homogeneity in the z-direction is mainly due to the boundary conditions of the $\lambda/2$-resonators, forming a half sine wave between the ends of the strip line. We restrict the sample to the central 2-D area of $100 \times 1000\ \mu m^2$, which has (100 μm above the resonator) a homogeneity of approximately 5×10^{-2}. We will refer to this area as the 'uniform region'. In general the width (y-direction) of this uniform region is

* Corresponding author at: Institute for Quantum Computing, Waterloo, ON, Canada. Fax: +1 519 888 7610.
E-mail address: obenning@uwaterloo.ca (O.W.B. Benningshof).

1090-7807/$ - see front matter © 2013 Elsevier Inc. All rights reserved.
http://dx.doi.org/10.1016/j.jmr.2013.01.010

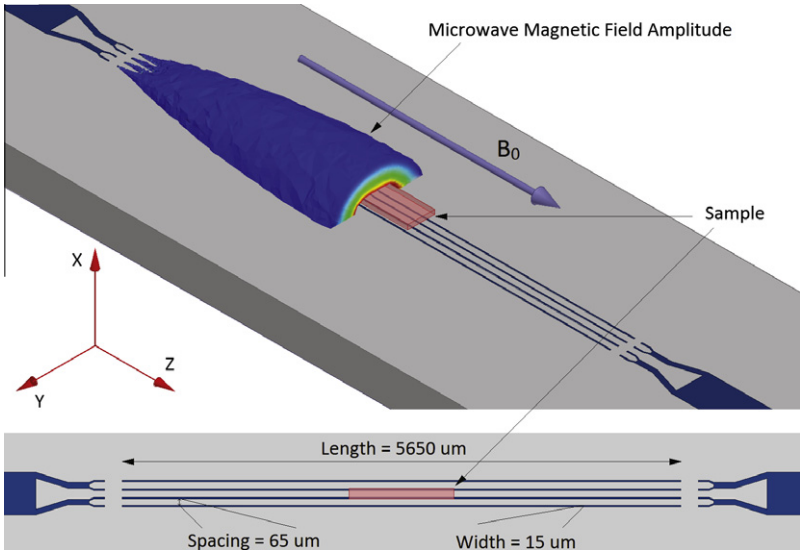

Fig. 1. The device consists of four parallel $\lambda/2$ microstrip line resonators, which are separated by 65 μm. One $\lambda/2$-resonator is 5650 μm long, 15 μm wide and 200 nm thick. It is structurized on a 430 μm thick sapphire wafer, which has a Nb ground plane on the underside. The sample is placed on top and in the center of the resonator. It is excited by a microwave magnetic field B_1. Because of symmetry only one half of the amplitude of the microwave magnetic field is shown, so that the resonator structure and the sample position are visible. When the thin film is placed in the uniform region (square in topview figure) the B_1 field is mainly determined by its y-component. The static magnetic field is applied along the z-axis, which enables pulsed ESR in a thin film. We have fabricated resonators with up to 16 parallel striplines.

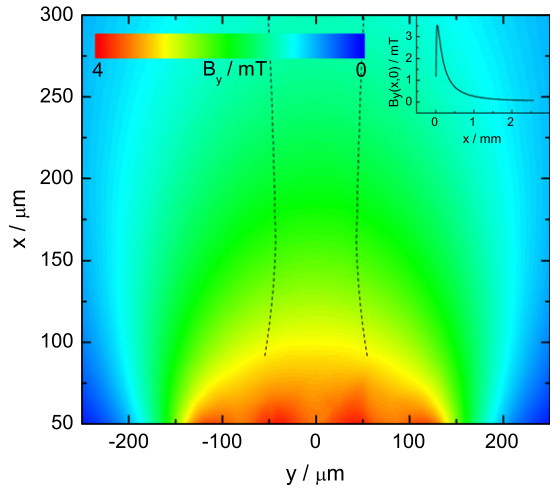

Fig. 2. The simulated profile of B_y above the middle of the microstrip resonator when excited by a 50 Ω source providing 1 W. Spatial variation in the magnetic field is large near the surface of the substrate but reduces continuously for higher levels such that good uniform magnetic fields are achieved 100 μm above the resonator. Between the dashed-lines (width of roughly 100 μm) the field homogeneity $|B_y(x,y) - B_y(x,0)|/|B_y(x,0)|$ is less than 5×10^{-2}. In the sub-figure (top right corner) is plotted how $B_y(x,0)$ varies with height above the center of the resonator. Between 60 μm and 700 μm the magnetic field strength is in very good agreement with an exponential decay with a characteristic length of roughly 210 μm.

determined by the number of parallel $\lambda/2$-resonators. This width is roughly 100, 400 and 800 μm for 4, 8 and 16 parallel $\lambda/2$-resonators, respectively. The magnetic field strength in the volume above the resonator (x-direction) is in very good agreement with an exponential decay between 60 μm and 700 μm. After 700 μm the magnetic field strength drops typically as $x^{-3/2}$, see Fig. 2.

Our devices were fabricated by sputtering a 200 nm thick layer of Niobium (Nb) on both sides of a C-orientated sapphire substrate with a thickness of 430 μm, patterned by photolithography and followed by reactive ion etching using sulfur hexafluoride (SF_6). The resulting device measured 0.3×1.3 cm^2 and was mounted in the middle of a top-plated microstrip line carrier printed circuit board (PCB) by silver paint to ensure thermal and electrical anchoring. The device and PCB are connected by aluminum wire bonds and all are enclosed in a copper package with two SMA connectors.

Superconducting resonators can obtain a Q of $\sim 10^5$ for 10 GHz [13,14] at the lowest temperatures. Here the Q is determined by the external losses ($\propto 1/Q_E$) and the intrinsic losses ($\propto 1/Q_I$), hence $1/Q = 1/Q_E + 1/Q_I$. As the intrinsic losses are strongly temperature dependent the Q increases for lower temperatures. The Q of the resonator used in the experiments (all performed at 4.2 K) described below is 1500.

For optimal power transfer the resonator has to be critically coupled to the transmission lines, controlled by adjusting the size of the gap between the strips and the fingers of the power splitter to match the external losses Q_E to the intrinsic losses Q_I. The observed power transfer during our performed experiments was approximately 10%, yielding a gap size of 150 μm for optimal power transfer at LHe temperatures. Because the Q_I is temperature dependent, the gap should be adjusted for a specific temperature in order to achieve critical coupling. In studies to explore the Q_I temperature behavior we used large gaps (150 μm) and observed Q's as high as 29,000 at 250 mK in the absence of a static external field.

The bulk critical field of Nb ($H_{c_2}(0) \approx 500$ mT and $H_{c_2}(4.2) \approx 300$ mT [15]) is close to the $B_0 (\sim 350$ mT) used for the ESR experiments. However, nanostructured Nb [16] increases the critical H_{c_2} significantly, which further increases as the substrate is mounted parallel to the applied magnetic field B_0 [17]. Having a lower reduced-field ($H/H_{c_2}(0) \approx 0.1$) will only moderately change the properties of the resonator (Q and ω_r) with respect to zero field.

3. Strong coupling effects

In the past few years several groups have reported strong coupling effects with an ensemble of microscopic emitters to a superconducting resonator. Examples, all coupled to a CPW resonator, include transmon-type superconducting qubits [5,6], electron-spins in solids [7], and spins in rare earth ions [8] or NV centers [9–11]. Here we demonstrate magnetic strong coupling of the microstrip resonator with an ensemble of electron spins. The

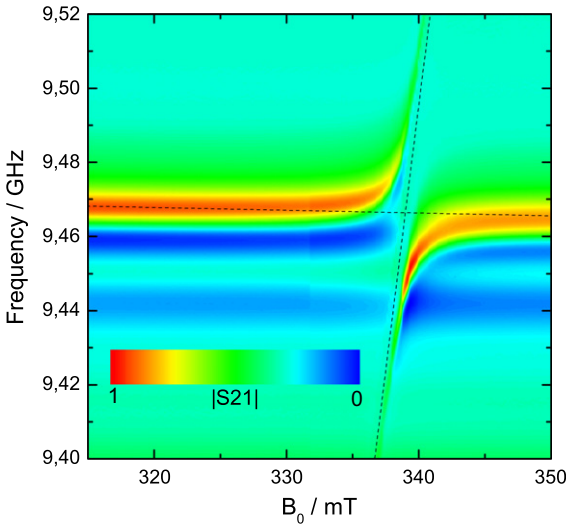

Fig. 3. Normalized transmission $|S_{21}|$ as a function of magnetic field at 4.2 K. Dashed lines indicate the bare resonator and electron frequencies. The frequency of the resonator slightly shifts under the influence of the increasing magnetic field. The avoided crossing of the coupled resonator spin-ensemble is observed at $\omega_0 = \omega_r$, which yields a vacuum Rabi splitting of $41.6\text{MHz} = 2 \cdot G_{ens}/2\pi$. Due to line resonances in the transmission lines, some artifacts are visible in the background.

ensemble consist of the stable free radicals of PTM, which have a g-factor of 2.0026 [18].

Tavis and Cummings [19] analyzed the coupling of N identical two level systems to a single-mode quantized radiation field. They showed that with a coupling g_j of every individual electron with the resonator the collective interaction of the ensemble scales with $\sqrt{N}$, hence $G_{ens} = g_j\sqrt{N}$. The strong coupling regime is entered when $G_{ens} \gg \kappa, \gamma$, where κ and γ are the resonator and emitter damping rates, respectively. The generalized collective coupling constant [8,7,10] for a homogeneous distribution of the electron spin density ρ is given by:

$$G_{ens} = \frac{g\mu_B}{2\hbar}\sqrt{\zeta\eta\mu_0\hbar\omega_r\rho}, \tag{1}$$

where $\zeta = \left(\frac{n_\uparrow - n_\downarrow}{n_\uparrow + n_\downarrow}\right)$ is the relative electron spin-polarization. The filling factor η in the uniform region is given by $\eta = \int |B_y(\vec{r})|^2 dV_{sample} / \int (|\vec{B}_1(\vec{r})|^2) dV$.

Typically, strong coupling effects in CPW resonators are achieved with $\sim 10^{12}$ microscopic emitters. However, the characteristic mode volume of CPW structures is roughly 10–100 times smaller than for microstrip structures. To compensate, and considered that G_{ens} should be larger than $\kappa/2\pi \approx 6.8$ MHz, we aimed for a polarized electron ensemble of $\sim 10^{15}$.

The crystals, with an approximated total volume of 6×10^{-11} m^3 ($\pm 3 \times 10^{-11}$ m^3), were placed in the middle of and 100 μm above the resonator (uniform region). The PTM crystal was formed as a clathrate with benzene [20] with a density of 1.3×10^{27} electron spins m^{-3}. This density provided us with an ensemble of 8×10^{16} electron spins. The resonator contained by the microwave package was cooled to LHe temperatures in a dewar with a superconducting magnet, resulting in a spin polarization near resonance of 6%. The setup was connected to two copper semi-rigid coax cables from LHe temperatures to an Agilent N5230A PNA-L network analyzer. The S-parameters were measured while the magnetic field was slowly ramped. The normalized results of the $|S_{21}|$ are displayed in Fig. 3.

The calculated collective coupling constant from Eq. (1) is $G_{ens}/2\pi = 21.8$ MHz (where η is estimated to be approximately 4×10^{-3}), which agrees with our observations of the vacuum Rabi splitting to within 5%. The coupling constant for a single electron is then $g_j/2\pi = 0.30$ Hz. As expected, this is two orders of magnitude lower than the coupling for a typical CPW resonator measurement, due to the higher mode volume for the microstrip resonator.

4. Nutation spectroscopy

We also used the microstrip resonator to obtain a 1-D ESR image (or projection) of the electron spin density of a bulk sample. This allowed us to study the uniformity and the spatial mapping of the B_1 field. As the magnetic field drops very nearly exponentially above the $\lambda/2$-resonators, the Rabi spectrum is a 1-D image of the electron spin density. Our experiment is based on the 2-D NMR study of near-surface regions of conductors by Skibbe and Neue [21]. In their case the B_1 falls off due to the skin effect in the conductors.

A fit of our simulations yields a field above the resonator that drops as $B_y(x) = VAe^{-x/\lambda}$ between 60 and 700 μm, where V is the pulse voltage, $A = 0.24$ mT/V and λ is the characteristic length of 210 μm. For a bulk sample placed on top of the resonator all electron spins at any height (x) will experience a field $B_y(x)$. Consequently, the electrons in a sheet parallel to the resonator plane will experience the same magnetic field. Thus, the Rabi frequency varies with sample height above the resonator.

The simplest pulsed ESR experiment consists of a single pulse, however, the ring down time (Q/ω_r) for the resonator is comparable to the relaxation time T_2^* of our system [22]. In this case it is more convenient to record a spin-echo [23]. The pulse sequence is $t_p - \tau - t_p - t_2$, where t_p is the pulse length, τ the dephasing time, and t_2 the acquisition time, during which the echo is recorded.

In a uniform field the echo intensity from two identical pulses is $\sin(\theta)\sin^2(\frac{\theta}{2})$, where θ is the nutation angle [24]. The echo intensity is easiestly understood as an integral of the echo response over the spin density $\rho(x)$ above the resonator. The contribution of the spins depends on their position relative to the resonator. By the principle of reciprocity [25] the contribution of the spins scales as the distribution of $B_y(x)$ over the sample, hence $e^{-x/\lambda}$.

$$S(V) \propto \int \rho(x) e^{-x/\lambda} \sin(\gamma_e B_y(x) t_p) \sin^2\left(\frac{\gamma_e B_y(x) t_p}{2}\right) dx, \tag{2}$$

where γ_e is the electron gyromagnetic ratio, 1.7608×10^{11} rad s^{-1} T^{-1}. It is convenient to rewrite the integral using the identity $\sin(\theta)\sin^2(\frac{\theta}{2}) = \frac{1}{2}\sin(\theta) - \frac{1}{4}\sin(2\theta)$. We then see that the signal corresponds to the sum of two Fourier encodings:

$$S(V) \propto \int \frac{\rho(x)}{2} e^{-x/\lambda} \sin(\gamma_e B_y(x) t_p) dx - \int \frac{\rho(x)}{4} e^{-x/\lambda} \sin(2\gamma_e B_y(x) t_p) dx. \tag{3}$$

Following Skibbe and Neue we rescale the spatial coordinate as a logarithm since $B_y(x) = VAe^{-x/\lambda}$,

$$S(V) \propto -\frac{\lambda}{2}\int \rho(-\lambda \ln(x')) \sin(2\pi v_1(x')V) dx' + \frac{\lambda}{4}\int \rho(-\lambda \ln(x')) \sin(4\pi v_1(x')V) dx', \tag{4}$$

where $2\pi v_1 = \gamma_e A t_p x'$. Here we see that in the case where $B_y(x)$ drops exponentially over the sample (for non-linear functions the number of spins per interval $B_y(x)$ increases with decreasing slope) it exactly cancels out the damped signal of the spins due to their position, as already observed by Skibbe and Neue. The Fourier transform reveals:

$$\mathcal{F}_V[S(V)] \propto \frac{\lambda}{4i}\frac{2\pi}{\gamma_e A t_p}\rho(-\lambda \ln(x')) - \frac{\lambda}{8i}\frac{2\pi}{\gamma_e A t_p}\rho(-\lambda \ln(x'/2)). \tag{5}$$

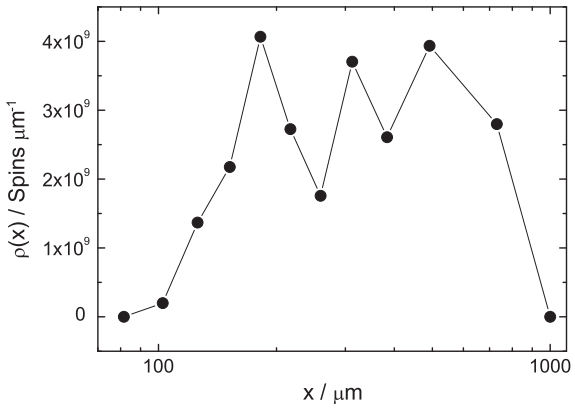

Fig. 4. 1-D spectrum of the Si:P sample. The crystal has an uniform electron density, therefore its irregular shape shows up in the 1-D image.

We use nutation spectroscopy with echo readout to map the spin density as a function of height above the resonator.

In order to determine the spin density distribution $\rho(x)$ from the Fourier spectrum, we have to make a correction. As shown in Eq. (5), the Fourier transform contains two copies of the image with Nyquist frequencies that differ by a factor of 2. We suppress the second component by starting from the lowest frequency and adding it to the amplitude of the higher frequency.

Si:P with a phosphorus doping concentration of $\sim 10^{17}$ P/cm^3 is a convenient sample as the T_1 is shorter than 1 s [26] at LHe temperatures. Due to hyperfine splitting at these temperatures [27] one of the electron spin resonance lines in the experiment is matched to the resonance frequency of the resonator. The irregular shaped crystal, with approximate dimensions of $0.3 \times 1.8 \times 0.7$ mm^3 ($W \times L \times H$), was placed in the middle of the resonator and lifted 100 μm with a Kapton spacer.

The spectrometer is a home-built X-band pulsed ESR system. The pulse length t_p was kept fixed at 100 ns during all of the experiments with an echo time τ of 1.4 μs. The variation in pulse strength was controlled by varying (in 20 steps) the pulse voltage between zero and 20 V (corresponding to a B_1 of ~3 mT at 100 μm). Each spectrum is the average of 64 scans with 10 s in between. Fig. 4 shows the observed spin density as a function of height above the resonator and resonance frequency for the Si:P sample.

5. Conclusion

The high-Q and uniform field over a broad 2-D region of the micro-stripline cavity presented in this work enables X-band pulsed ESR studies of thin film samples. In addition to providing a spectroscopic tool for chemistry and materials science of thin films, the described device may find application in planar multinode designs for a quantum information processor [28–30]. To verify the performance of the resonator, we demonstrated nutation spectroscopy depth probing of a Si:P sample and strong coupling to an organic radical spin ensemble with a coupling constant for a individual electron spin of $g_j/2\pi = 0.30$ Hz.

Acknowledgments

We thank T.W. Borneman for assisting us with the pulsed ESR spectroscopy. This research was undertaken, in part, thanks to funding from the Canada Excellence Research Chairs Program. The infrastructure used for this work would not be possible without the significant contributions of the Canada Foundation for Innovation, the Ontario Ministry of Research & Innovation and Industry Canada. Their support is gratefully acknowledged.

References

[1] T.W. Borneman, D.G. Cory, J. Magn. Reson. 225 (2012) 120.
[2] R. Narkowicz, D. Suter, R. Stonies, J. Magn. Reson. 175 (2005) 275.
[3] R. Narkowicz, D. Suter, I. Niemeyer, Rev. Sci. Instrum. 79 (2008) 084702.
[4] H. Malissa, D.I. Schuster, A.M. Tyryshkin, A.A. Houck, S.A. Lyon, 2012, arXiv:1202.6305.
[5] J.M. Fink, R. Bianchetti, M. Baur, M. Göppl, L. Steffen, S. Filipp, P.J. Leek, A. Blais, A. Wallraff, Phys. Rev. Lett. 103 (2009) 083601.
[6] A. Imamoglu, Phys. Rev. Lett. 102 (2009) 083602.
[7] D.I. Schuster, A.P. Sears, E. Ginossar, L. DiCarlo, L. Frunzio, J.J.L. Morton, H. Wu, G.A.D. Briggs, B.B. Buckley, D.D. Awschalom, R.J. Schoelkopf, Phys. Rev. Lett. 105 (2010) 140501.
[8] P. Bushev, A.K. Feofanov, H. Rotzinger, I. Protopopov, J.H. Cole, C.M. Wilson, G. Fischer, A. Lukashenko, A.V. Ustinov, Phys. Rev. B 84 (2011) 060501.
[9] T. Duty, Physics 3 (2010) 80.
[10] Y. Kubo, F.R. Ong, P. Bertet, D. Vion, V. Jacques, D. Zheng, A. Dréau, J.-F. Roch, A. Auffeves, F. Jelezko, J. Wrachtrup, M.F. Barthe, P. Bergonzo, D. Esteve, Phys. Rev. Lett. 105 (2010) 140502.
[11] R. Amsüss, C. Koller, T. Nöbauer, S. Putz, S. Rotter, K. Sandner, S. Schneider, M. Schramböck, G. Steinhauser, H. Ritsch, J. Schmiedmayer, J. Majer, Phys. Rev. Lett. 107 (2011) 060502.
[12] Ansoft Corporation, Pittsburgh, PA, Ansoft HFSS, Version 13.0.2, 2011.
[13] A.J. DiNardo, J.G. Smith, F.R. Arams, J. Appl. Phys. 42 (1971) 186.
[14] J. Zmuidzinas, Ann. Rev. Condens. Matter Phys. 3 (2012) 169.
[15] K. Saito, KEK Accelerator Lab, Ibaraki-ken, in: 10th International SRF Workshop, Japan, 2001.
[16] S. Bose, P. Raychaudhuri, R. Banerjee, P. Ayyub, Phys. Rev. B 74 (2006) 224502.
[17] M. Tinkham, Introduction to superconductivity, Dover Books on Pysics and Chemistry, Dover Publications, 2004.
[18] M. Ballester, J. Riera-Figueras, J. Castaner, C. Badfa, J.M. Monso, J. Am. Chem. Soc. 93 (1971) 2215.
[19] M. Tavis, F.W. Cummings, Phys. Rev. 170 (1968) 379.
[20] J. Veciana, J. Carilla, C. Miravitlles, E. Molins, J. Chem. Soc. Chem. Commun. 812 (1987).
[21] U. Skibbe, G. Neue, Colloids Surf. 45 (1990) 235.
[22] A. Schweiger, G. Jeschke, Principles of Pulse Electron Paramagnetic Resonance, Oxford University Press, 2001.
[23] G. Rinard, R. Quine, S. Eaton, G. Eaton, W. Froncisz, J. Magn. Reson., Ser. A 108 (1994) 71.
[24] A. Sodickson, D.G. Cory, Prog. Nucl. Magn. Reson. Spectrosc. 33 (1998) 77.
[25] D.I. Hoult, N.S. Ginsberg, J. Magn. Reson. 148 (2001) 182.
[26] G. Feher, E.A. Gere, Phys. Rev. 114 (1959) 1245.
[27] G. Feher, E.A. Gere, Phys. Rev. 103 (1956) 501.
[28] L. Jiang, J.M. Taylor, A.S. Srensen, M.D. Lukin, Phys. Rev. A 76 (2007) 062323.
[29] M. Mehring, J. Mende, Phys. Rev. A 73 (2006) 052303.
[30] T.W. Borneman, C.E. Granade, D.G. Cory, Phys. Rev. Lett. 108 (2012) 140502.